Nonlinear Dyn (2012) 67:227–249
DOI 10.1007/s11071-011-9974-9

ORIGINAL PAPER

Nonlinear analysis of the dynamics of articulated composite rotor blades

Mehrdaad Ghorashi

Received: 6 April 2010 / Accepted: 3 February 2011 / Published online: 2 March 2011

Abstract The general nonlinear intrinsic equations of motion of an elastic composite beam are solved in order to obtain the elasto-dynamic response of a rotating articulated blade. The solution utilizes the linear Variational-Asymptotic Method (VAM) cross-sectional analysis, together with an improved damped nonlinear model for the rigid-body motion analysis of helicopter blades in coupled flap and lead-lag motions. The explicit (direct) integration algorithm implements the perturbation method in order to solve the transient form of the nonlinear intrinsic differential equations of motion and obtain the elasto-dynamic behavior of an accelerating composite blade. The specific problem considered is an accelerating articulated helicopter blade of which its motion is analyzed since it starts rotating from rest until it reaches the steady-state condition. It is observed that the steady-state solution obtained by this method compares very well with other available solutions. The resulting simulation code is a powerful tool for analyzing the nonlinear response of composite rotor blades; and for serving the ultimate aim of efficient noise and vibration control in helicopters.

M. Ghorashi (✉)
Department of Engineering, University of Southern Maine, Gorham, ME, USA
e-mail: mghorashi@usm.maine.edu

Keywords Articulated blades · Intrinsic equations of a beam · Accelerating helicopter blade · Steady-state solution · Variational Asymptotic Method (VAM)

Nomenclature

A	cross-sectional area of the undeformed beam in x_2–x_3 plane
e_1	$[1 \quad 0 \quad 0]^T$
F_i	elements of the column matrix of internal forces
f	applied forces per unit length
g	determinant of the metric tensor in curvilinear coordinates
H	sectional angular momenta
i_2, i_3	cross-sectional mass moment
i_{23}	cross-sectional product of inertia
$K.E.$	kinetic energy function
K	deformed beam curvature vector $= k + \bar{\kappa}$
k	undeformed beam curvature vector
l	length of the beam
M_i	elements of the column matrix of internal moments
m	applied moments per unit length
N	number of nodes
P	sectional linear momenta
S	stiffness matrix
t	time
V	velocity field
x_i	global system of coordinates
x_1	axis along the beam
x_2 and x_3	cross-sectional axes

$\bar{x}_2$ and $\bar{x}_3$	offsets from the reference line of the cross-sectional mass center
γ	$[\gamma_{11} \quad 2\gamma_{12} \quad 2\gamma_{13}]^T$
Δ	identity matrix
$\delta\bar{q}$	virtual displacement vector
$\delta\bar{\psi}$	virtual rotation vector
κ_1	elastic twist
κ_i	elastic bending curvatures ($i = 2, 3$)
μ	mass per unit length
ρ	mass density
Ω	angular velocity
$(\breve{\bullet})$	perturbations in space
$(\hat{\bullet})$	perturbations in time
$(\bullet)'$	$\frac{\partial(\bullet)}{\partial x_1}$
$(\dot{\bullet})$	$\frac{d(\bullet)}{dt}$
$(\delta\bar{\bullet})$	overbar indicates that it need not be the variation of a functional
$(\hat{\bullet})$	the discrete boundary value of quantity $(\bullet)$
$(\breve{\bullet})_{ij}$	$-e_{ijk}(\bullet)_k$
$\langle\bullet\rangle$	$\int_A (\bullet)\, dx_2\, dx_3$
$\langle\langle\bullet\rangle\rangle$	$\langle(\bullet)\sqrt{g}\rangle = \int_A (\bullet)\sqrt{g}\, dx_2\, dx_3$, $\sqrt{g} = 1 - x_2 k_3 - x_3 k_2$

1 Introduction

Helicopter, with its capability of vertical take-off and landing is a crucial means of aerial transportation. The expansion of the domain of application of helicopters, however, has been hampered by a few serious constraints. Among them is the relatively poor ride quality associated with high levels of vibration and noise. Vibration can result in a low fatigue life of structural components, and hence, increase the operating costs. Furthermore, noise and vibration have severe environmental consequences that have limited the range of application and the velocity of helicopters. Reducing noise and vibration is a major goal in the design of next generation helicopters. Achieving this aim, however, requires the development of the necessary and numerically efficient analytical and simulation tools.

Analysis of blade models can be developed using three dimensional (3-D) finite-elements method (FEM) models. However, modeling initially twisted and curved active rotor blades using 3-D FEM is extremely expensive. Also, for preliminary design and for control synthesis, this approach is quite computationally intensive. As an alternative, a helicopter rotor blade can be modeled as a slender composite beam. The beam model of a helicopter blade is deemed to be an efficient alternative [16].

In the past two decades, research has been focused on the analysis of anisotropic composite beams using the Variational-Asymptotic Method (VAM)—an excellent review of which can be found in Hodges [15]. VAM, as a powerful method for solving a variety of beam problems, was first introduced in Berdichevsky [1]. Using it is computationally more efficient than preparing a complete 3-D model of the beam. VAM starts from the elastic energy functional of the beam. It solves problems that can be formulated as minimization of a functional (e.g. finding the stationary points for the energy functional) and have an inherently small dimension (e.g. beams, plates and shells). The solution has the common advantage of asymptotic methods of being mathematically well-grounded with no ad hoc assumptions about displacement or stress fields [15]. Interestingly, there are no theoretical restrictions on the geometry of the cross section or on the materials of the beams for which VAM can be applied. It is especially proper for realistic modeling of initially curved and twisted anisotropic beams (like rotor blades).

VAM reduces the 3-D geometrically nonlinear elasticity problem of composite rotating blades to a nonlinear 1-D analysis involving the solution of the nonlinear intrinsic differential equations of motion of a beam along its span. This 1-D analysis utilizes the cross-sectional properties obtained by a 2-D analysis. The 2-D analysis results are the cross-sectional stiffness and mass matrices as well as the warping functions. These results are then used in all further 3-D analyses of the rotating blade without the need to repeat the 2-D analysis. VAM is ideal for simulating the response of helicopter rotor blades which are laterally flexible and usually operate in the nonlinear range [15].

VAM was applied, in Berdichevsky et al. [2], for the analysis of thin-walled closed anisotropic cross-section beams to obtain closed-form solution of the 4×4 stiffness matrix. Later, in Shang and Hodges [19], a nonlinear 1-D solution was performed and a solution for the intrinsic equations of a beam was presented. The obtained results were compared with the available experimental data given in Sharpe [20].

In Hodges et al. [14], VAM was used in order to analyze the response of initially curved and twisted composite beams. Solutions for the nonlinear static

deformation and the linear free vibration about the static state of deformation were presented. Results were compared with the published exact solutions for isotropic beams and also with available experimental data for rotating isotropic and composite beams with swept tips. In both cases, good correlations were observed.

For certain simple cases like isotropic beams with relatively simple cross-sectional geometries, the stiffness constants can be calculated in closed form. For complex cross-sections made of composites, however, a 2-D FEM discretization has been introduced which implements the VAM cross-sectional analysis and minimizes the 2-D elastic energy functional. This FEM code is called the *Variational Asymptotic Beam Sectional* Analysis program (VABS) and was introduced by Hodges et al. [13].

The implementation of actuator and sensor elements in beams in order to build smart beams generated new problems that have been tackled by Cesnik and his co-workers. In Cesnik and Shin [6], an asymptotic formulation for analyzing multi-cell composite helicopter rotor blades with integral anisotropic active plies was presented. This work includes both the cross-sectional and the 1-D analyses. In Cesnik and Ortega-Morales [3], the VAM 2-D analysis was applied to include the effect of an embedded active element in a structure. An extended version of the same paper is Cesnik and Ortega-Morales [4].

The results of the VAM cross-sectional analysis were validated in Yu et al. [21]. In this paper, VAM results for elliptical, channel and triangular prism bars, as well as box and I-beams were compared against other methods. Furthermore, it was demonstrated that although the application of VABS is restricted to beam problems, it provides a level of accuracy which is comparable to that of standard 3-D finite-element codes, but with far less computing and processing requirements.

In Yu and Hodges [22], VABS solutions were compared with those of the 3-D elasticity solution. Identical results were reported for beams with elliptical and rectangular cross sections. The authors concluded that VAM, which is the mathematical foundation of VABS, is a valid methodology and it can be used to avoid difficulties in dealing with 3-D elasticity; while obtaining results that are coincident with the exact solutions.

Recently, Ghorashi and Nitzsche [10] presented an implicit (indirect) structural algorithm to calculate the steady-state response of composite hingeless rotor blades. First the corresponding form of the intrinsic equations is obtained in the form of a boundary value problem. This problem is then converted into a series of initial value problems where the unknown initial conditions are calculated through an iterative process using the Newton–Raphson method. The solution is repeated and when a convergence criterion is satisfied, the correct solution of the boundary value problem and the steady-state response of the blade are obtained. In Ghorashi [11] and Ghorashi and Nitzsche [12], this method was extended to the dynamic analysis of hingeless rotating blades.

In the present paper, the method used in Ghorashi and Nitzsche [12] is applied to hinged rotating beams. First a review of the analysis of rigid articulated rotating blades having flap and lead-lag hinges is presented. The corresponding equations of motion are valid at constant rotor angular velocity and for the rectilinear motion of the helicopter. These equations are then expanded in order to include hinge offset, aerodynamics and nonlinear coupling. Next, the elastic articulated rotating blades are considered and their root boundary conditions are formulated by the solution of the rigid articulated blade. Having done that, the root boundary condition is used together with the elastic rotating blade formulation in order to solve the elastic articulated rotating blade problem. The numerical solution utilizes a finite-difference technique on both time and space domains for calculating the transient elastodynamic response.

2 Euler and extended Euler equations for rigid rotating blades

A typical hinge arrangement for an articulated blade is shown in Fig. 1. The use of these hinges in order to reduce the induced moments has been a main development in the manufacture of helicopters [7].

To analyze the dynamics of rigid articulated blades, Euler or Extended Euler equations can be utilized. For a rigid body which rotates about a fixed point O the moment equations of motion about O using a system of reference attached to the rigid body and coincident with its principal axes of inertia are well known to be

$$\sum M_x = I_{xx}\dot{\omega}_x - (I_{yy} - I_{zz})\omega_y\omega_z \tag{1}$$

$$\sum M_y = I_{yy}\dot{\omega}_y - (I_{zz} - I_{xx})\omega_z\omega_x \tag{2}$$

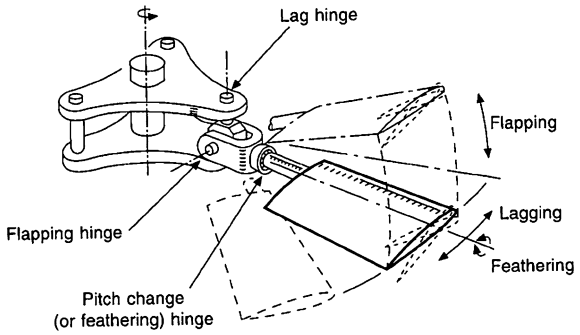

Fig. 1 Typical hinge arrangement [7]

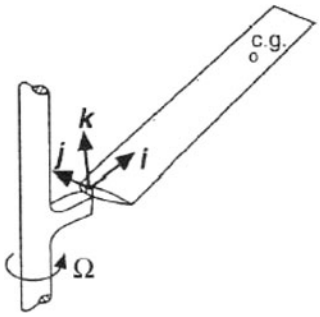

Fig. 2 Articulated blade having offset hinges [7, p. 363]

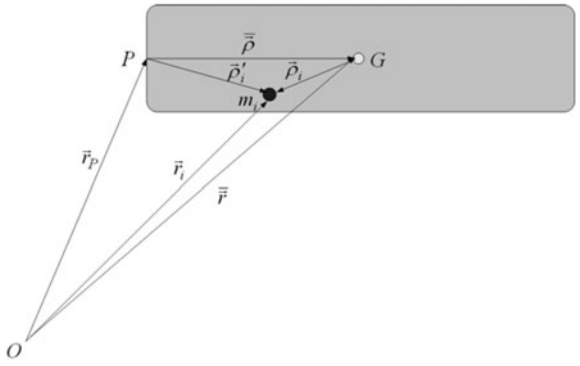

Fig. 3 Schematic presentation of the horizontal plane of Fig. 2 with O on the shaft axis and P at the hinge location at the root of the blade

$$\sum M_z = I_{zz}\dot{\omega}_z - (I_{xx} - I_{yy})\omega_x\omega_y \tag{3}$$

Equations (1)–(3) are the Euler's equation of motion for a rotating rigid body and are applicable to rotating articulated blades with no hinge offset.

For non-zero hinge offset illustrated in Fig. 2 and modeled in Fig. 3, the fixed point O (on the shaft of the rotor about which the blade rotates) is not on the hinge location P (at the root of the blade) and the hinge offset is OP. In this case, following the procedure given in Done and Balmford [7], the moment equations of motion about P using a system of reference attached to the rigid blade with center of gravity at

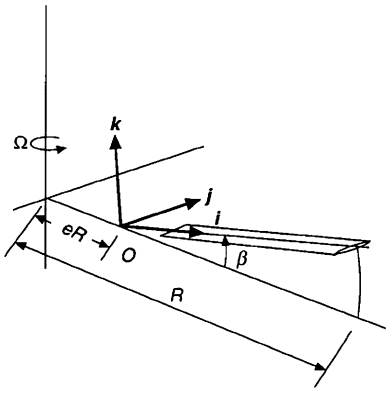

Fig. 4 Single flapping blade [7]

$$\overline{\overline{\rho}} = x_G\hat{i}, \qquad y_G = 0, \qquad z_G = 0 \tag{4}$$

and coincident with its principal axes of inertia would be

$$\sum M_{Px} = I_{xx}\dot{\omega}_x - (I_{yy} - I_{zz})\omega_y\omega_z \tag{5}$$

$$\sum M_{Py} = I_{yy}\dot{\omega}_y - (I_{zz} - I_{xx})\omega_z\omega_x - mx_G a_{Pz} \tag{6}$$

$$\sum M_{Pz} = I_{zz}\dot{\omega}_z - (I_{xx} - I_{yy})\omega_x\omega_y + mx_G a_{Py} \tag{7}$$

These are the 'extended' Euler equations adapted for the case of a rotating blade with hinge offset and can be used for deriving the equations of motion of a rigid articulated blade in flapping, lagging, and feathering.

3 Nonlinear coupled motions of rigid articulated blade

The blades of an articulated rotor have two primary degrees of freedom: flap and lead-lag, which can take place about their corresponding hinges. These hinges are used in order to reduce the root blade loads, since at the hinge moments must be zero.

3.1 Coupled flapping and lead-lag equation considering hinge offset

Figure 4 illustrates a rotating blade with a flap hinge mounted at distance eR from the axis of rotation. The

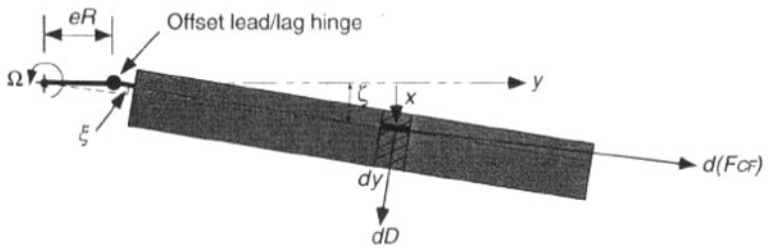

Fig. 5 Blade with an offset lead-lag hinge [18, p. 177]

coordinate system is attached to the blade with its origin at the hinge and the axes aligned with the principal directions of inertia of the blade. The flap angle β is measured relative to a plane perpendicular to the shaft axis and its positive sense is in the negative y direction (flapping up).

Figure 5 illustrates a lead-lag hinge. This hinge is parallel to the shaft axis and the lead-lag angle ξ represents a change of the blade angle in the plane of the hub. The positive direction of the lead-lag angle is defined as the one for a backward moving blade. Thus, the 'lagging' direction (opposite to the shaft angular velocity Ω) is considered positive.

If the lead-lag and the flap motions act at the same time, the angular velocity of the blade in the blade coordinate system would be

$$\vec{\omega} = (\Omega \sin\beta\cos\xi)\hat{i} + (\Omega \sin\beta \sin\xi - \dot{\beta})\hat{j} + (\Omega\cos\beta - \dot{\xi})\hat{k} \tag{8}$$

For constant Ω, depicted by Ω_{ss}, the acceleration of the hinge point P in the hub coordinate system can be transformed to the blade coordinate system resulting in

$$\vec{a} = eR\Omega^2(-\cos\beta\cos\xi\hat{i} - \cos\beta\sin\xi\hat{j} + \sin\beta\hat{k}) \tag{9}$$

Substituting (8) and (9) into (7), assuming β and ξ to be small to ignore the second-order terms, and using a mechanical lag damper result in

$$\ddot{\xi} + C_\xi\dot{\xi} + \nu_\xi^2\Omega^2\xi + 2\Omega\beta\dot{\beta} = -\frac{1}{I_{zz}}\sum M_{Pz}, \qquad \nu_\xi^2 = \frac{mx_{Gn}eR^2}{I_{zz}} \tag{10}$$

In (10) M_z is mainly provided by the drag forces.

To obtain the lag-coupled flap equation, (8) and (9) may now be substituted into (6). For small flap and lead-lag angles one obtains

$$\ddot{\beta} + \Omega^2\left(1 + \frac{mx_{Gn}eR^2}{I_{yy}}\right)\beta - \Omega(2\dot{\xi}\beta + \dot{\beta}\xi) = -\frac{1}{I_{yy}}\sum M_{Py} \tag{11}$$

This is a generalization of the following equation stated on pp. 394 and 653 of Johnson [17] and p. 197 of Leishman [18]:

$$\ddot{\beta} + \Omega^2\nu_\beta^2\beta - 2\Omega\dot{\xi}\beta = -\frac{1}{I_{yy}}\sum M_{Py}, \qquad \nu_\beta^2 = 1 + \frac{mx_{Gn}eR^2}{I_{yy}} \tag{12}$$

It should be noted that the flap and the lead-lag equations of motion (10) and (11) are nonlinearly coupled and linearizing decouples them. Using the azimuth angle of the blade as the independent variable, (10) and (11) would convert into

$$\frac{d^2\beta}{d\psi^2} + \left(1 + \frac{mx_{Gn}eR^2}{I_{yy}}\right)\beta - \left(2\beta\frac{d\xi}{d\psi} + \xi\frac{d\beta}{d\psi}\right) = -\frac{1}{\Omega^2 I_{yy}}\sum M_{Py} \tag{13}$$

$$\frac{d^2\xi}{d\psi^2} + \frac{C_\xi}{\Omega_{ss}}\frac{d\xi}{d\psi} + \left(\frac{mx_{Gn}eR^2}{I_{zz}}\right)\xi + 2\beta\frac{d\beta}{d\psi} = -\frac{1}{\Omega_{ss}^2 I_{zz}}\sum M_{Pz} \tag{14}$$

3.2 Case study: undamped rigid articulated blade in hover

Figure 6 illustrates a blade modeled as a prismatic member with a solid rectangular section made of a homogeneous isotropic material for which

$$A = 0.02\ \text{m}^2, \qquad \rho = 1770\ \text{kg/m}^3 \tag{15}$$

The hinge offset can be assumed to be

$$x_{Gn} = 0.48, \qquad e = 0.04, \qquad R = 1.04\ \text{m} \tag{16}$$

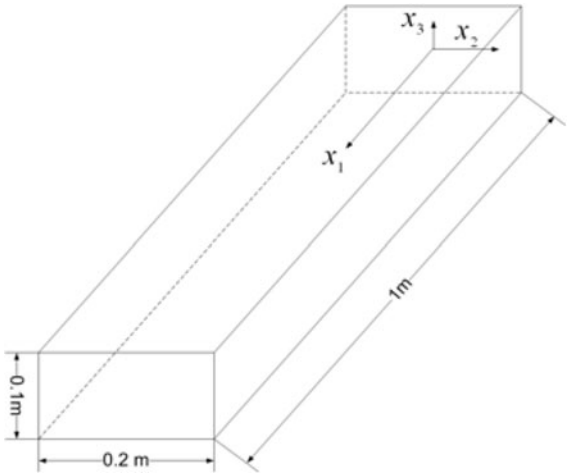

Fig. 6 The geometry of the rotating blade and the coordinate axes

For a steady-state shaft angular velocity of $\Omega_{ss} = 100$ rad/s and moments $M_y = -1000$ N m, $M_z = -10$ N m the coupled flap-lag equations without including the aerodynamic damping in flap and the mechanical damper in lead-lag would be

$$\ddot{\beta} + (100)^2(1 + 0.0621)\beta - 100(2\dot{\xi}\beta + \dot{\beta}\xi) = \frac{1000}{11.8295} \tag{17}$$

$$\ddot{\xi} + 0.0617 \times (100)^2\xi + 200\beta\dot{\beta} = \frac{10}{11.9180} \tag{18}$$

Figure 7 illustrates the results. In this figure, solutions of (17) and (18) are labeled, 'present'. The 'Leishman' label corresponds to the solution of (12) for the numerical values of the present case and the 'Uncoupled' solution is the solution of (17) and (18) when the three nonlinear terms are ignored. It is seen that the flap motion has a 1 per rev frequency, as expected, and the lead-lag response is much slower. In order to see the results more clearly, zoomed views have been plotted in Fig. 8.

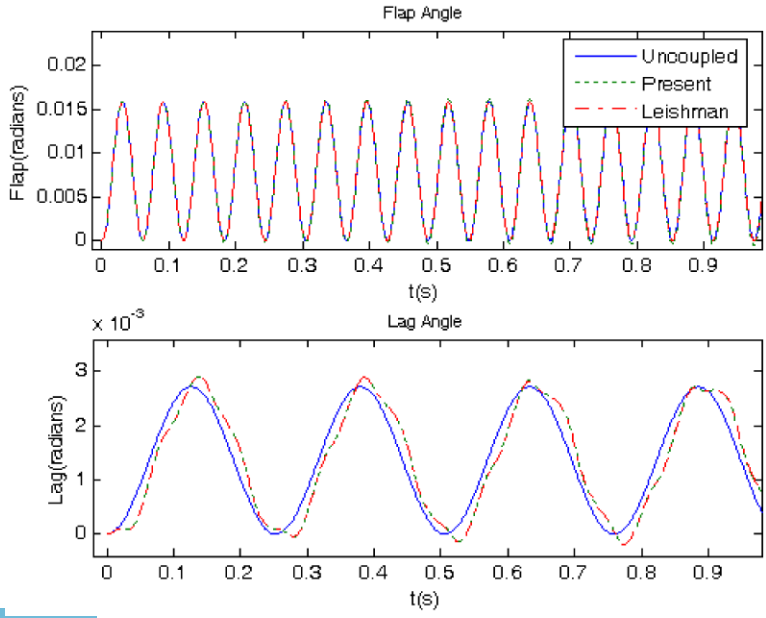

Fig. 7 Time history diagrams for lead-lag and flap motions

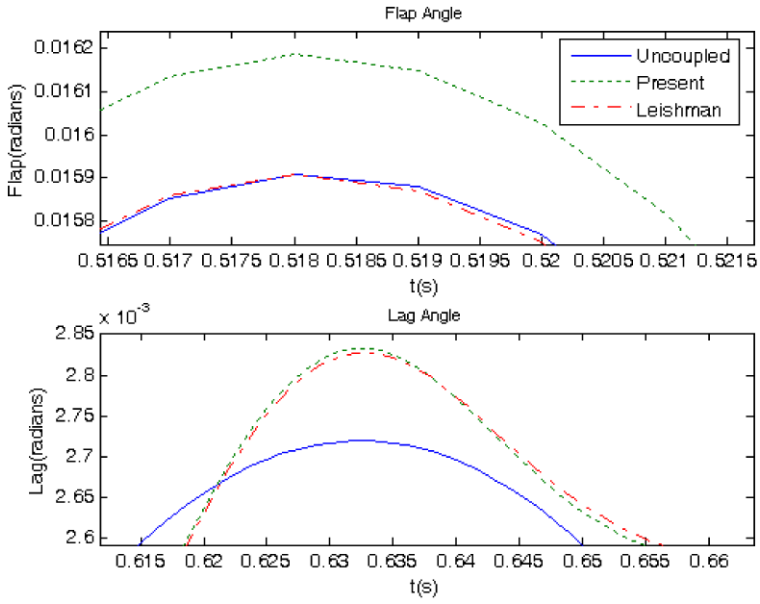

Fig. 8 Time history diagrams for lead-lag and flap motions (Fig. 7 zoomed)

4 Aerodynamic damping in rigid articulated blades

4.1 Aerodynamic damping effect

In forward flight, by ignoring the free-stream velocity and axial climbing, only the effects of blade pitch, flap motion and the induced velocity field would remain. Therefore, the lift force per unit length would be [18, p. 179]

$$L = \frac{1}{2}\rho U_T^2 c C_{L\alpha}\left(\theta - \frac{\dot{\beta} r}{U_T} - \frac{v_i}{U_T}\right) \tag{19}$$

Ignoring the hinge offset, and using the Lock number defined as

$$\gamma = \frac{\rho c C_{L\alpha} R^4}{I_{yy}} \tag{20}$$

The flapping equation with pitch and aerodynamics would be

$$\frac{d^2\beta}{d\psi^2} + \left(\frac{\gamma}{8}\right)\frac{d\beta}{d\psi} + \beta = \frac{\gamma}{8}\left(\theta - \frac{4\lambda_i}{3}\right) \tag{21}$$

4.2 Hinge offset effect on aerodynamically damped flap motion

So far the contributions of hinge offset and aerodynamic forces on the flap motion have been considered separately. Now, the combined effect of these two factors on this motion is studied. Recalling (13) and (20) and utilizing

$$-\sum M_{Py} = \int_{eR}^{R} L(r - eR)\, dr \tag{22}$$

One obtains

$$\begin{aligned}\frac{d^2\beta}{d\psi^2} &+ \left(\frac{\gamma}{8}(1-e)^3\left(1+\frac{1}{3}e\right)\right)\frac{d\beta}{d\psi} \\ &+ \left(1 + \frac{m x_{Gn} e R^2}{I_{yy}}\right)\beta - \left(2\beta\frac{d\xi}{d\psi} + \xi\frac{d\beta}{d\psi}\right) \\ &= \frac{\gamma}{2}\left[\left(\frac{1}{4} + \frac{1}{12}e^4 - \frac{1}{3}e\right)\theta\right. \\ &\left. - \left(\frac{1}{3}\left(1-e^3\right) - \frac{1}{2}e\left(1-e^2\right)\right)\lambda_i\right]\end{aligned} \tag{23}$$

Equation (23), when linearized for the especial case of zero offset reduces to (21) and for zero cyclic pitch or induced velocity reduces to

$$\frac{d^2\beta}{d\psi^2} + \left[\frac{1}{8}\gamma(1-e)^3\left(1+\frac{1}{3}e\right)\right]\frac{d\beta}{d\psi} + (1+\varepsilon)\beta = 0 \tag{24}$$

which is given in Done and Balmford [7].

So, (14) and (23) are the general set of flap and lead-lag equations of motion where the effects of hinge offset, aerodynamic damping and nonlinear coupling have all been taken into account.

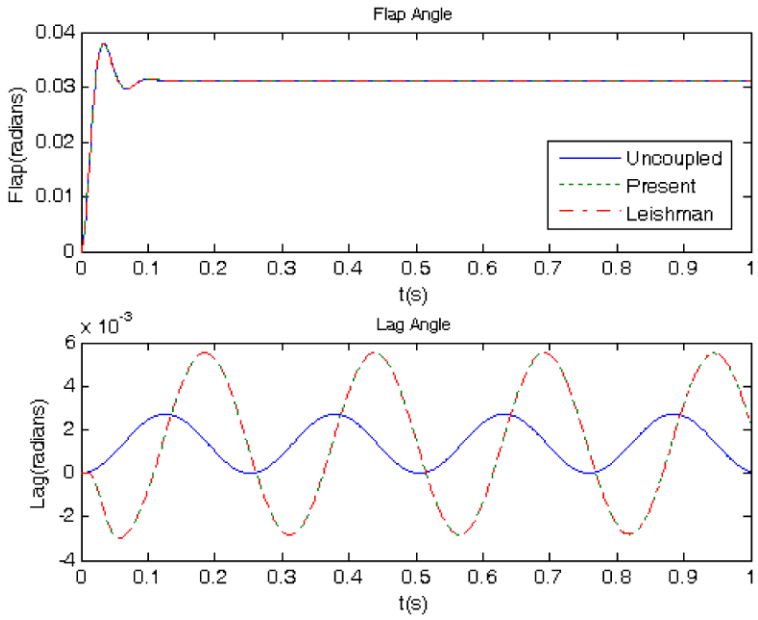

Fig. 9 Time history diagrams of flap and lead-lag with aerodynamic damping included

4.3 Case study: articulated blade model with aerodynamic damping

Using (14) and (23), and recalling the case study given in Sect. 3.2 with $\gamma = 8$, and a collective pitch angle of 2°, the set of nonlinear flap and lead-lag equations of motion become,

$$\ddot{\beta} + 89.6\dot{\beta} + (100)^2(1 + 0.0621)\beta - 100(2\dot{\xi}\beta + \dot{\beta}\xi) = 330.45 \tag{25}$$

$$\ddot{\xi} + 0.0617 \times (100)^2\xi + 200\beta\dot{\beta} = \frac{10}{11.9180} \tag{26}$$

Figure 9 illustrates the solution where the effect of damping on the flap motion and the formation of the coning angle are evident. It is seen, however, that the effect of aerodynamic damping of the flap motion is not significant on the lead-lag motion. Figure 10 illustrates a zoomed view of Fig. 9.

To control the lead-lag motion, mechanical dampers can be implemented. The equations of motion would then be modified as

$$\ddot{\beta} + 89.6\dot{\beta} + (100)^2(1 + 0.0621)\beta - 100(2\dot{\xi}\beta + \dot{\beta}\xi) = 330.45 \tag{27}$$

$$\ddot{\xi} + 10\dot{\xi} + 0.0617 \times (100)^2\xi + 200\beta\dot{\beta} = \frac{10}{11.9180} \tag{28}$$

Figures 11 and 12 illustrate the corresponding solution where the damping effect on both motions is evident.

5 Elastic analysis using the variational asymptotic method

Having analyzed the dynamics of rigid articulated blades, the next step is the inclusion of elasticity in the analysis. To this end, using the logic of the Variational Asymptotic Method (VAM), a nonlinear elastic 1-D analysis along the rotating blade is needed which utilizes the results of the cross-sectional analysis (performed by VABS). This analysis implements the following equations.

5.1 Intrinsic equations of motion

For a blade modeled as a generalized Timoshenko beam, application of the Hamilton's principle results in Hodges [15]

$$\int_{t_1}^{t_2}\int_0^L \{\delta\bar{q}^T(F' + \tilde{K}F + f - \dot{P} - \tilde{\Omega}P) + \delta\bar{\psi}^T[M' + \tilde{K}M + (\tilde{e}_1 + \tilde{\gamma})F + m - \dot{H} - \tilde{\Omega}H - \tilde{V}P]\}\,dx_1\,dt$$

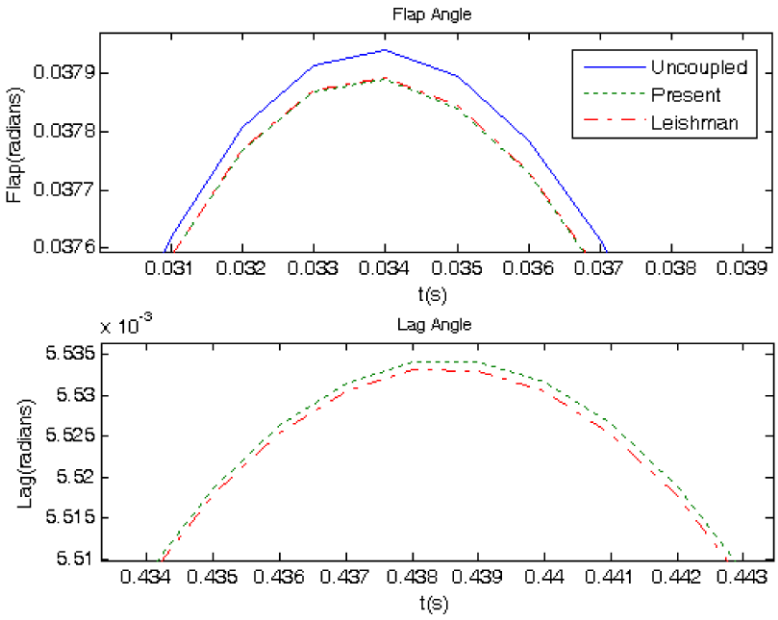

Fig. 10 Time history diagrams of flap and lead-lag with aerodynamic damping included (Fig. 9 zoomed)

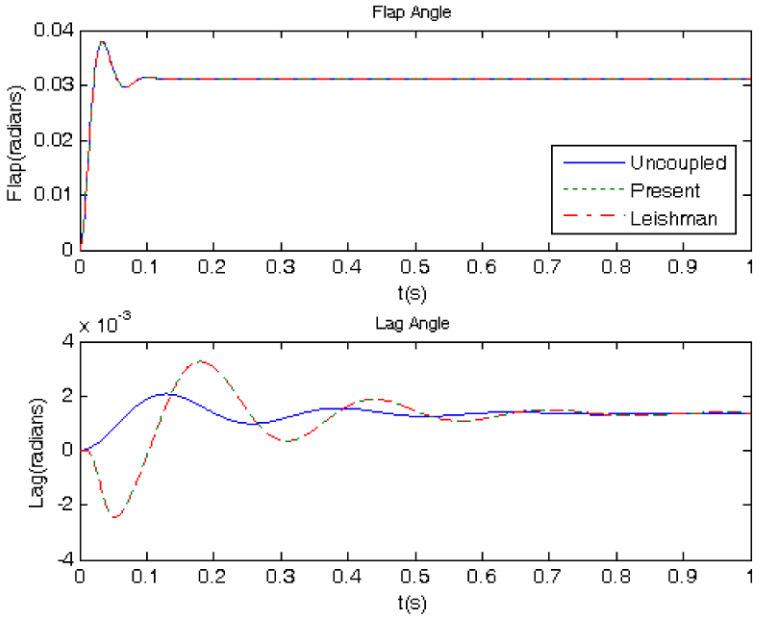

Fig. 11 Time history diagrams of flap and lead-lag with aerodynamic damping and lead-lag dampers included

$$= \int_0^L \left[\delta\bar{q}^T(\hat{P}-P) + \delta\bar{\psi}^T(\hat{H}-H)\right]\Big|_{t_1}^{t_2} dx_1 - \int_{t_1}^{t_2} \left[\delta\bar{q}^T(\hat{F}-F) + \delta\bar{\psi}^T(\hat{M}-M)\right]\Big|_0^L dt \tag{29}$$

The corresponding Euler–Lagrange equations are

$$F' + \tilde{K}F + f = \dot{P} + \tilde{\Omega}P \tag{30}$$

$$M' + \tilde{K}M + (\tilde{e}_1 + \tilde{\gamma})F + m = \dot{H} + \tilde{\Omega}H + \tilde{V}P \tag{31}$$

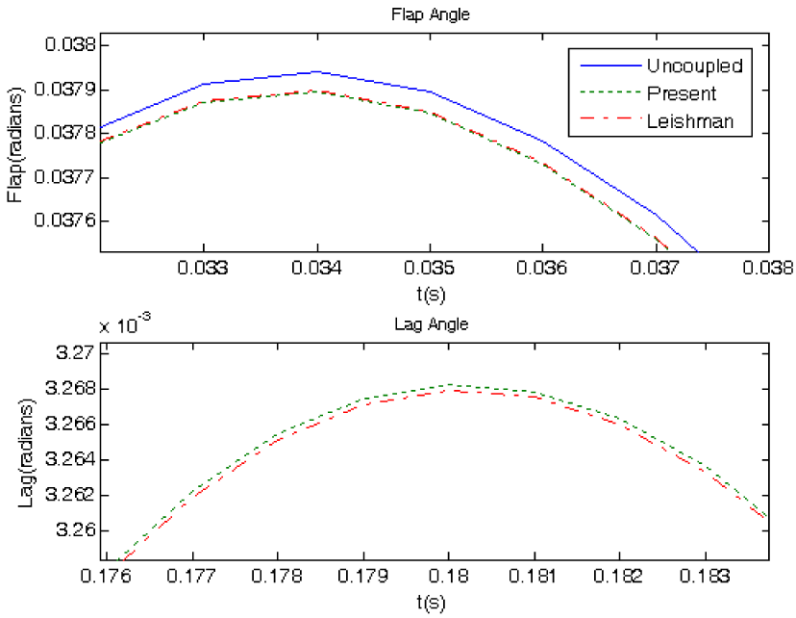

Fig. 12 Time history diagrams of flap and lead-lag with aerodynamic damping and lead-lag dampers included (Fig. 11 zoomed)

where the total curvature and twist of the blade is the summation of their initial values and the added curvature and twist as a result of elastic deformation,

$$K = k + \kappa \tag{32}$$

Equations (30) and (31) are the nonlinear intrinsic equations of motion of a beam. Here, F and M are column vectors of internal forces and moments, respectively. The first element of F is the axial force and the second and third elements are the shear forces, expressed in the deformed beam basis. Similarly, the first element of M is the twisting moment and the second and third elements are bending moments.

The generalized sectional linear and angular momenta P and H are conjugate to motion variables by derivatives of the kinetic energy function,

$$P = \left(\frac{\partial K.E.}{\partial V}\right)^T \tag{33}$$

$$H = \left(\frac{\partial K.E.}{\partial \Omega}\right)^T \tag{34}$$

5.2 Intrinsic kinematical equations

The nonlinear intrinsic kinematical equations of a beam that should be solved together with (30) and (31) are [15]

$$V' + \tilde{K}V + (\tilde{e}_1 + \tilde{\gamma})\Omega = \dot{\gamma} \tag{35}$$

$$\Omega' + \tilde{K}\Omega = \dot{\kappa} \tag{36}$$

5.3 Momentum-velocity equations

The momentum-velocity equations are [15]

$$\begin{Bmatrix} P \\ H \end{Bmatrix} = \begin{bmatrix} \mu\Delta & -\mu\tilde{\bar{\xi}} \\ \mu\tilde{\bar{\xi}} & i \end{bmatrix} \begin{Bmatrix} V \\ \Omega \end{Bmatrix} \tag{37}$$

where

$$\xi = \begin{Bmatrix} 0 \\ x_2 \\ x_3 \end{Bmatrix} \tag{38}$$

$$\tilde{\bar{\xi}} = \begin{bmatrix} 0 & -\bar{x}_3 & \bar{x}_2 \\ \bar{x}_3 & 0 & 0 \\ -\bar{x}_2 & 0 & 0 \end{bmatrix} \tag{39}$$

also

$$i = \langle\langle \rho(\xi^T \xi.\Delta - \xi\xi^T) \rangle\rangle = \begin{bmatrix} i_2 + i_3 & 0 & 0 \\ 0 & i_2 & i_{23} \\ 0 & i_{23} & i_3 \end{bmatrix} \tag{40}$$

and

$$\mu = \langle\langle \rho \rangle\rangle = \langle \rho\sqrt{g} \rangle \tag{41}$$

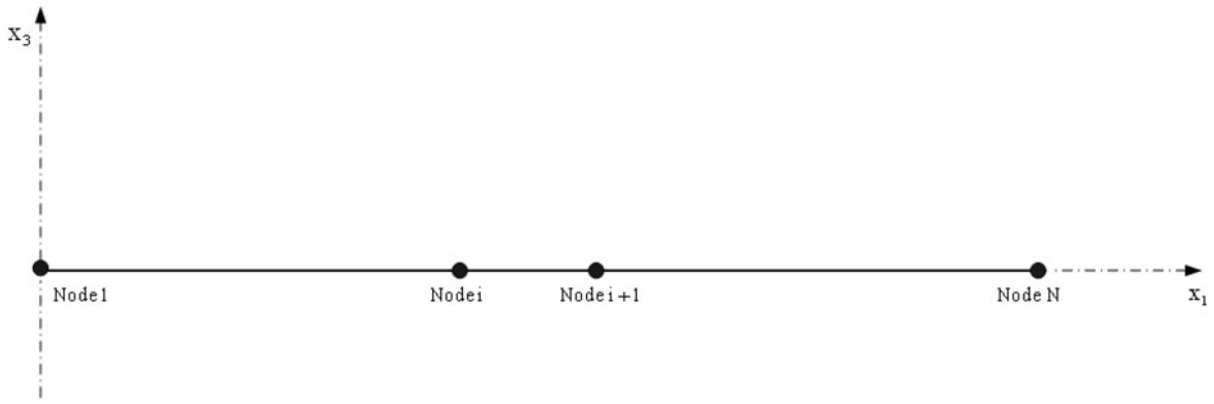

Fig. 13 Nodes along the blade and the coordinate system of the undeformed blade

where

$$\langle(\bullet)\rangle = \int_A (\bullet)\, dx_2\, dx_3 \tag{42}$$

and g is the determinant of the metric tensor, expressible as

$$\sqrt{g} = 1 - x_2 k_3 - x_3 k_2 \tag{43}$$

5.4 Constitutive equations

The 2-D analysis performed by VABS results in the warping functions as well as the stiffness matrix used in the constitutive equations,

$$\begin{Bmatrix} \gamma \\ \kappa \end{Bmatrix} = \underbrace{\begin{bmatrix} R & Z \\ Z^T & T \end{bmatrix}}_{S^{-1}} \begin{Bmatrix} F \\ M \end{Bmatrix} \tag{44}$$

$$\begin{Bmatrix} F \\ M \end{Bmatrix} = \underbrace{\begin{bmatrix} A & B \\ B^T & D \end{bmatrix}}_{S} \begin{Bmatrix} \gamma \\ \kappa \end{Bmatrix} \tag{45}$$

Equations (30), (31), (32), (35), (36), (37) and (44) form a system of four nonlinear partial differential equations and five linear vector equations. They have a total of nine unknown vectors: F, M, V, Ω, P, H, γ, κ, and K, at every node along the beam and every time step. In what follows, these equations are solved using finite differences in time and space, as well as the perturbations method.

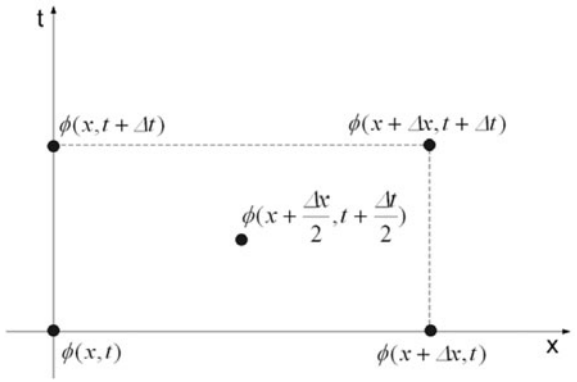

Fig. 14 The time–space grid for the numerical solution of a partial differential equation

6 Formulation of the generic nonlinear term

Figure 13 illustrates the blade which is discretized by N nodes along its span. The corresponding finite-difference space-time grid presentation is depicted in Fig. 14. For a generic variable $\phi(x, t)$, one may use the following convention:

$$\phi_i = \phi(x, t) \tag{46}$$

where i is the beam node number corresponding to the position x. At the nodes neighboring (x, t) in Fig. 14, the same variable can be expressed as

$$\phi_{i+1} = \phi(x + \Delta x, t) \tag{47}$$

$$\phi_i^+ = \phi(x, t + \Delta t) \tag{48}$$

$$\phi_{i+1}^+ = \phi(x + \Delta x, t + \Delta t) \tag{49}$$

where the superscript "+" refers to the next time step.

Using Taylor series expansions,

$$\phi\left(x+\frac{\Delta x}{2},t+\frac{\Delta t}{2}\right) = \phi\left(x,t+\frac{\Delta t}{2}\right)+\phi'\left(x,t+\frac{\Delta t}{2}\right)\times\frac{\Delta x}{2} \quad (50)$$

$$\phi\left(x,t+\frac{\Delta t}{2}\right)=\phi(x,t)+\dot{\phi}(x,t)\times\frac{\Delta t}{2} \quad (51)$$

and the notation introduced in (46) to (49) one obtains

$$\phi\left(x+\frac{\Delta x}{2},t+\frac{\Delta t}{2}\right) = \frac{1}{4}\left(\phi^+_{i+1}+\phi^+_i+\phi_{i+1}+\phi_i\right)+O\left(\Delta x^2,\Delta t^2\right) \quad (52)$$

$$\phi'\left(x+\frac{\Delta x}{2},t+\frac{\Delta t}{2}\right) = \frac{1}{2\Delta x}\left(\phi^+_{i+1}-\phi^+_i+\phi_{i+1}-\phi_i\right)+O\left(\Delta x^2,\Delta t^2\right) \quad (53)$$

$$\dot{\phi}\left(x+\frac{\Delta x}{2},t+\frac{\Delta t}{2}\right) = \frac{1}{2\Delta t}\left(\phi^+_{i+1}-\phi_{i+1}+\phi^+_i-\phi_i\right)+O\left(\Delta x^2,\Delta t^2\right) \quad (54)$$

Equations (52) to (54) provide second-order approximate finite-difference expressions for a variable and its derivatives with respect to time and space. They have been used in Ghorashi [9] and Esmailzadeh and Ghorashi [8] to solve a moving load problem. In what follows, (52) to (54) will be used in order to convert the system of nonlinear partial differential equations (30), (31), (35) and (36) into a set of difference equations.

Consider a generic nonlinear vector term $\tilde{\phi}\lambda$ with the scalar terms $\phi_m\lambda_n$ ($m=1:3$, $n=1:3$). One may use perturbations in time and space in order to express them in terms of the nodal values of variables ϕ_m and λ_n. For the perturbations in space,

$$\phi^+_{m,i+1}=\phi^+_{m,i}+\breve{\phi}_{m,i+1} \quad (55)$$

Similarly, for the perturbations in time,

$$\phi^+_{m,i}=\phi_{m,i}+\widehat{\phi}_{m,i} \quad (56)$$

Therefore,

$$\phi_m\lambda_n=\frac{1}{16}\left(3\phi_{m,i}+2\widehat{\phi}_{m,i}+\breve{\phi}_{m,i+1}+\phi_{m,i+1}\right)\times\left(3\lambda_{n,i}+2\widehat{\lambda}_{n,i}+\breve{\lambda}_{n,i+1}+\lambda_{n,i+1}\right) \quad (57)$$

For small perturbations, (57) reduces to

$$\phi_m\lambda_n=\frac{1}{16}\times\left[\left(\phi^+_{m,i+1}+\phi^+_{m,i}\right)\left(\lambda_{n,i+1}+3\lambda_{n,i}\right)+\left(\lambda^+_{n,i+1}+\lambda^+_{n,i}\right)\left(\phi_{m,i+1}+3\phi_{m,i}\right)\right]+\frac{1}{16}\times\left(\phi_{m,i+1}\lambda_{n,i+1}+\phi_{m,i+1}\lambda_{n,i}+\phi_{m,i}\lambda_{n,i+1}-3\phi_{m,i}\lambda_{n,i}\right) \quad (58)$$

Equation (58) is the equation for the generic nonlinear term.

7 The finite-difference formulation

Using (58) for all of the nonlinear terms in (30), (31), (35) and (36), one obtains

$$A_i q^+_i+B_i q^+_{i+1}=J_i \quad (59)$$

where the right-hand side of (59) contains the currently known quantities, and the column state vector q has 24 elements:

$$q=[F_1\ F_2\ F_3\ M_1\ M_2\ M_3\ V_1\ V_2\ V_3\ \Omega_1\ \Omega_2\ \Omega_3\ P_1\ P_2\ P_3\ H_1\ H_2\ H_3\ \gamma_{11}\ 2\gamma_{12}\ 2\gamma_{13}\ \kappa_1\ \kappa_2\ \kappa_3]^T \quad (60)$$

A_i and B_i are 24×24 matrices and q_i and J_i are column vectors. Expressions for A_i, B_i and J_i have been given in the appendices of Ghorashi [11] and Ghorashi and Nitzsche [12].

Equation (59) is composed of 24 algebraic equations with 48 unknowns and as such it is not solvable on its own. To solve the problem, one should utilize initial and boundary conditions as was done for a similar formulation in Ghorashi [9] and Esmailzadeh and Ghorashi [8]. Using (59),

$$q^+_1=M^{\text{tot}}_{N-1}.q^+_N+T^{\text{tot}}_{N-1} \quad (61)$$

where

$$M_{N-1}^{\text{tot}} = a_1 a_2 a_3 a_4 \ldots a_{N-1}, \quad a_i = -A_i^{-1} B_i$$
$$T_{N-1}^{\text{tot}} = b_1 + a_1 b_2 + a_1 a_2 b_3 + \cdots + a_1 a_2 a_3 \ldots a_{N-2} b_{N-1}, \quad b_i = A_i^{-1} J_i \tag{62}$$

If the boundary conditions at the two nodes 1 and N are known, one can then solve (61) for the remaining unknowns at these two nodes. Then, (59) can be used to provide the solution at all of the interior nodes.

8 Elastic articulated composite rotating blade

In Sects. 4 to 7 the behavior of rigid articulated blades as well as formulating a solution algorithm for the analysis of elastic rotating blades were discussed. The stage is now set for the analysis of elastic articulated blades. While for a rigid blade one can calculate the flap and lead-lag motions by solving the set of two coupled nonlinear differential equations, the same is not easily achievable for elastic blades. The main problem is that instead of having a purely initial value problem, one should solve a combined initial and boundary value problem whose root boundary conditions depend on the unknown solution of the differential equations of motion.

In this paper, in order to circumvent the mentioned problem, the angular velocity boundary conditions of the elastic blade at its root are taken from the corresponding solution for its rigid articulated blade counterpart. Therefore, first the rigid-body motions of lead-lag and flap are obtained by using rigid-body dynamics of the blade. Then these motions are utilized for calculating the angular velocity boundary conditions of the elastic blade at its root. Having done that, the stage would be set for solving the nonlinear elastic problem of the rotating blade using the perturbation method discussed before.

The logic behind this modeling lies in the fact that elastic deformations are much smaller than rigid-body motions. Therefore, root motion (which provides the boundary conditions for the blade) can be calculated by ignoring elastic deformations and momentarily assuming that the blade is rigid.

8.1 Solution algorithm for the nonlinear analysis of elastic articulated blades

Combining the algorithms for analyzing the rigid articulated blade and the elastic hingeless blade problems generates an algorithm which is suitable for analyzing elastic articulated blades. The solution for the motion of the blade would then be performed in the following steps.

Step 1: In this step the elastic blade, initially modeled as hingeless, is accelerated from rest to its full speed (the steady-state speed).

Step 2: The blade continues to rotate at full speed and experiences a steady-state condition while its root is still clamped. The purpose of this part is to obtain an idea of the stability of the response of the blade after the acceleration phase and before the aerodynamic loads are applied and the hinges are activated.

Step 3: While the blade is still rotating at full speed, the flap and lead-lag hinges are activated and at the same time the blade is subjected to aerodynamic loadings. To simulate this phase of motion, first the rigid-body code is run and the flap and lead-lag solutions are calculated by solving (14) and (23). Then the angular velocity components of the root of the elastic blade can be obtained by (8). Having obtained this important unknown, one may apply the blade boundary conditions into (61) to get,

$$\begin{Bmatrix} F^+ \\ M^+ \\ \begin{Bmatrix} 0 \\ eR\Omega_{ss} \\ 0 \end{Bmatrix} \\ \begin{Bmatrix} \Omega_{ss}\sin\beta\cos\xi \\ \Omega_{ss}\sin\beta\sin\xi - \dot{\beta} \\ \Omega_{ss}\cos\beta - \dot{\xi} \end{Bmatrix} \\ \begin{Bmatrix} 0 \\ \mu eR\Omega_{ss} \\ 0 \end{Bmatrix} \\ \begin{Bmatrix} (i_2+i_3)\Omega_{ss}\sin\beta\cos\xi \\ i_2(\Omega_{ss}\sin\beta\sin\xi - \dot{\beta}) \\ i_3(\Omega_{ss}\cos\beta - \dot{\xi}) \end{Bmatrix} \\ \gamma^+ \\ \kappa^+ \end{Bmatrix}_1$$

$$= M_{N-1}^{\text{tot}} \begin{Bmatrix} 0 \\ 0 \\ V^+ \\ \Omega^+ \\ P^+ \\ H^+ \\ 0 \\ 0 \end{Bmatrix}_N + T_{N-1}^{\text{tot}} \tag{63}$$

Equation (63) should now be solved for the remaining unknowns at the two nodes. Having obtained the boundary unknowns at nodes 1 and N, one may now use (59) in order to calculate the unknowns at all interior nodes, by starting from either node 1 or node N. Choosing node N as the starting point in order to march toward node 1, the following may be used:

$$q_i^+ = -A_i^{-1} B_i q_{i+1}^+ + A_i^{-1} J_i \tag{64}$$

or,

$$q_i^+ = a_i q_{i+1}^+ + b_i \tag{65}$$

In this way, having already obtained q_N^+ using (65), one may calculate q_{N-1}^+ and then continue to find q_{N-2}^+ and so on until eventually another approximate solution for q_1^+ is obtained. This result may then be compared with the q_1^+ calculated by (61) to check the accuracy of the solution procedure and the impact of round-off errors.

8.2 Case study: elastic articulated blade in hover

The blade discussed in Sects. 3.2 and 4.3 is now analyzed when it is modeled as an elastic part. To obtain parameters of the elastic model first using VABS the inertia and flexibility matrices are calculated as follows:

$$i = \begin{bmatrix} 8.333 & 0 & 0 \\ 0 & 1.6667 & 0 \\ 0 & 0 & 6.6667 \end{bmatrix} \times 10^{-5} \times 1770 \tag{66}$$

$$S = \begin{bmatrix} 0.358 \times 10^{12} & 0 & 0 & 0 & 0 & 0 \\ 0 & 0.1373 \times 10^{12} & 0 & 0 & 0 & 0 \\ 0 & 0 & 0.1074 \times 10^{12} & 0 & 0 & 0 \\ 0 & 0 & 0 & 0.354 \times 10^{9} & 0 & 0 \\ 0 & 0 & 0 & 0 & 0.298 \times 10^{9} & 0 \\ 0 & 0 & 0 & 0 & 0 & 0.119 \times 10^{10} \end{bmatrix} \tag{67}$$

The blade is assumed to have a hinge offset ratio of $e = 0.04$ and a steady-state shaft angular velocity of 100 rad/s. The accelerating part of the motion lasts for 0.5 s, during which the blade is still clamped at its root and it accelerates to full speed. The second part of the motion lasts for 0.1 s in which the blade continues to rotate at the steady-state speed while the root is still clamped. Finally, in the last 0.5 s of the motion, while the blade is still rotating at its full speed, the flap and lead-lag hinges are activated and at the same time the blade is subjected to two moment pulses in flap and lead-lag directions. One moment corresponds to the application of a collective pitch and the second one represents the drag force in the lead-lag motion.

The corresponding equations of motion for the rigid-body motion of the blade in flap and lead-lag would be

$$\ddot{\beta} + 89.6\dot{\beta} + (100)^2(1 + 0.0621)\beta - 100(2\dot{\xi}\beta + \dot{\beta}\xi) = 0.0845 \tag{68}$$

$$\ddot{\xi} + 0.0617 \times (100)^2 \xi + 200\beta\dot{\beta} = 0.0839 \tag{69}$$

The lead-lag motion here has no mechanical damper. Using the solution of (68) and (69) in the algorithm discussed in Sect. 8, the complete elasto-dynamic solution of the elastic articulated blade problem has been obtained and illustrated in Figs. 15–22.

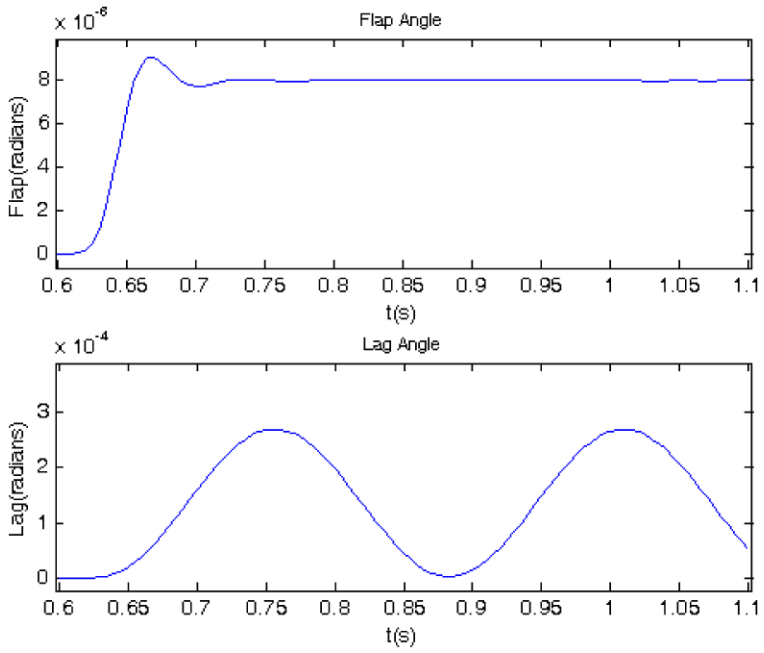

Fig. 15 Time history diagrams of lead-lag and flap motions

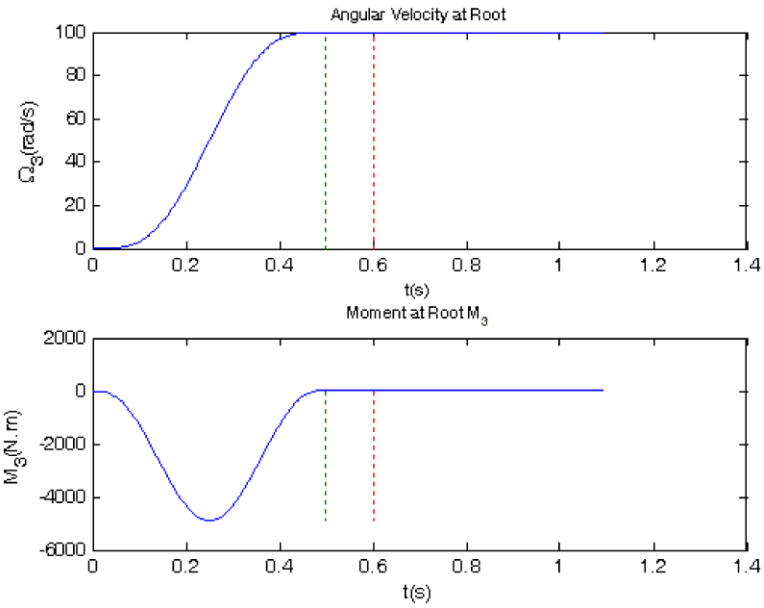

Fig. 16 Time history diagrams of shaft angular velocity and the M_3 bending moment induced in the blade at its root

The flap and lead-lag motions have been plotted in Fig. 15. This figure reveals that even though the flap and lead-lag motions are coupled, imposing damping on the flap motion only has negligible effect on the lead-lag motion.

The gentle variations of the root angular velocity and the resulting root moment and shear force can be seen in Fig. 16. As expected, maximum dynamic moment and shear force values occur when the angular acceleration of the blade is maximal.

The moment diagrams in Fig. 17 illustrate the induced moments at the root of the blade after activating the hinges. The values are seen to be small and always oscillating around zero. This is an indication of the ac-

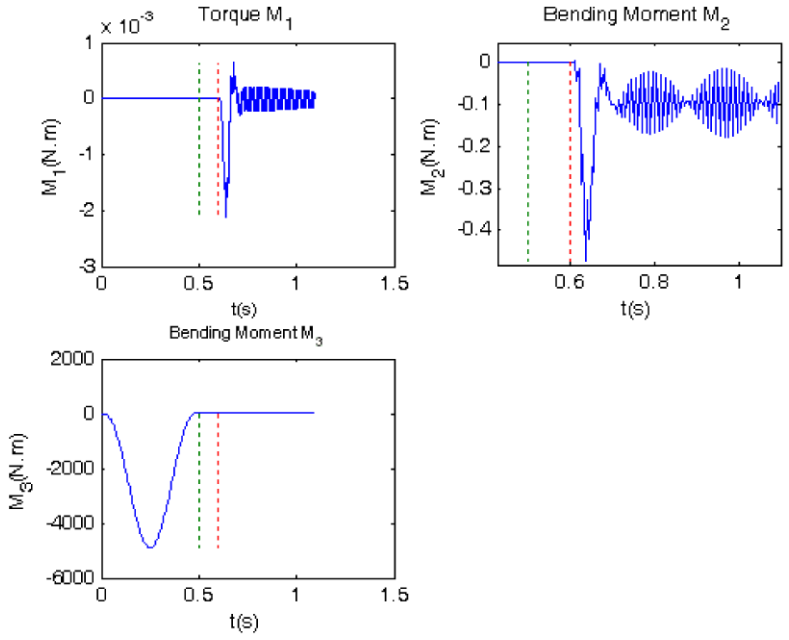

Fig. 17 Time history diagrams of blade internal moments components at its root

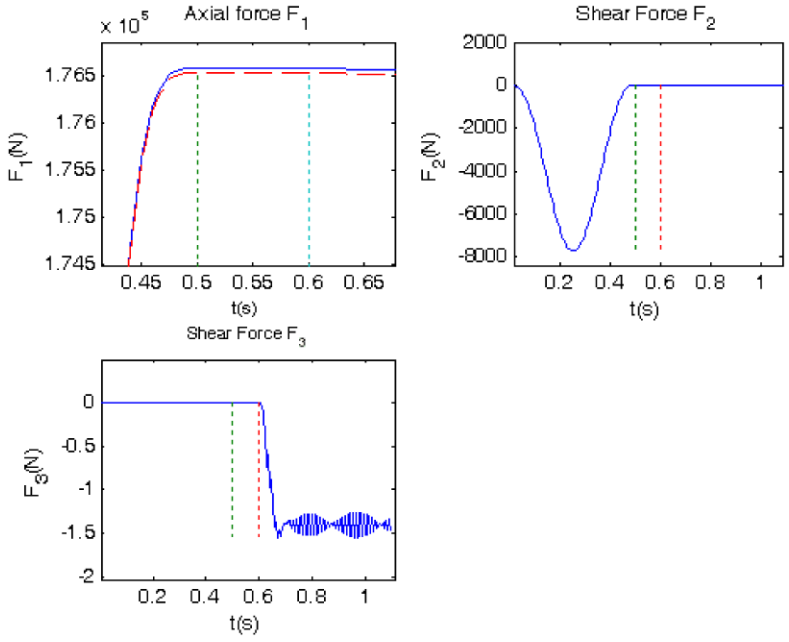

Fig. 18 Time history diagrams of blade internal force components at its root. The obtained result for F_1 (*solid line*) and the linear solution in (70) (*dashed line*)

curacy of the solution and the correct hinge modeling. This check point provides a very important verification tool and is an effective benchmark.

Figure 18 illustrates the time history diagram of the induced internal forces at the root of the blade. It can be observed that the obtained result for F_1 (solid line) is very close to that of the approximate solution

$$F_1 = \frac{1}{2}\rho A \Omega_3^2 \left(L^2 - x_1^2\right) \tag{70}$$

which is plotted as a dashed line.

In Fig. 19, the time history diagrams of various components of angular velocity are illustrated. Among

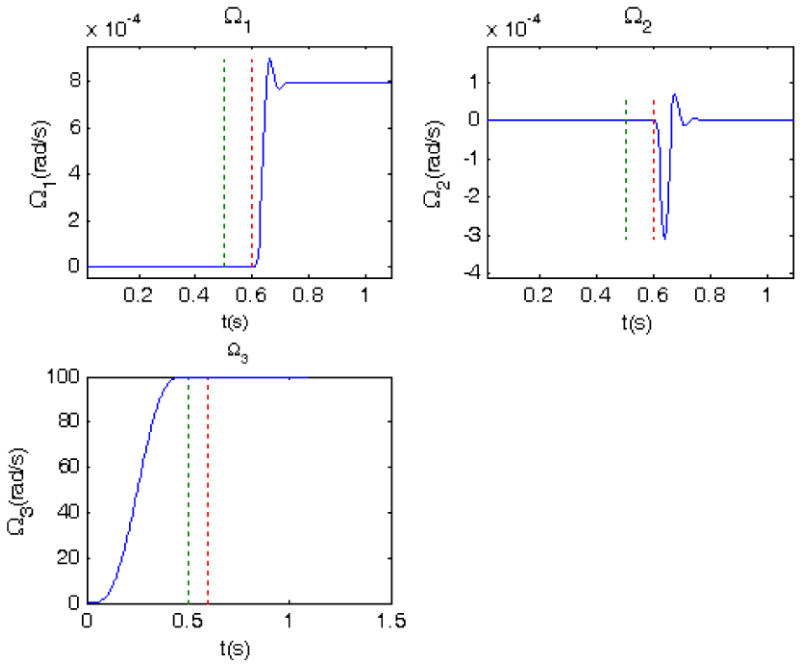

Fig. 19 Time history diagrams of blade angular velocity components at its root

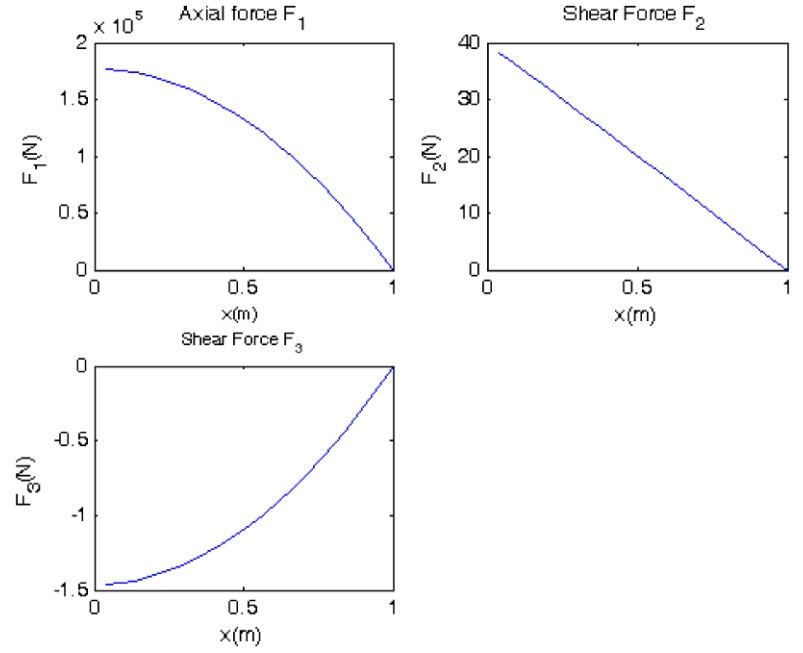

Fig. 20 Variation of blade internal force components along its span at $t = 0.85$ s

them, the convergence of Ω_2 to zero corresponds to the convergence of the flap angle to a constant which is the coning angle.

The variation of the internal forces, induced moments and angular velocities along the span of the blade at $t = 0.85$ s (while hinges are active) are plotted in Figs. 20, 21 and 22, respectively. Figure 20 shows that the major force generated along the blade is due to the centrifugal force. Also, in Figs. 20 and 21, the free boundary conditions at the tip of the blade are observed to have been satisfied, as expected.

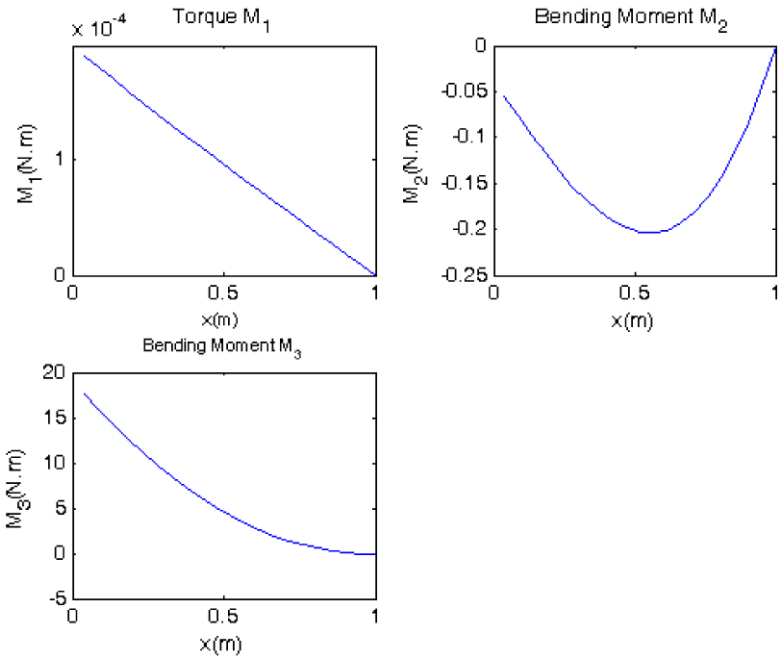

Fig. 21 Variation of blade internal moment components along its span at $t = 0.85$ s

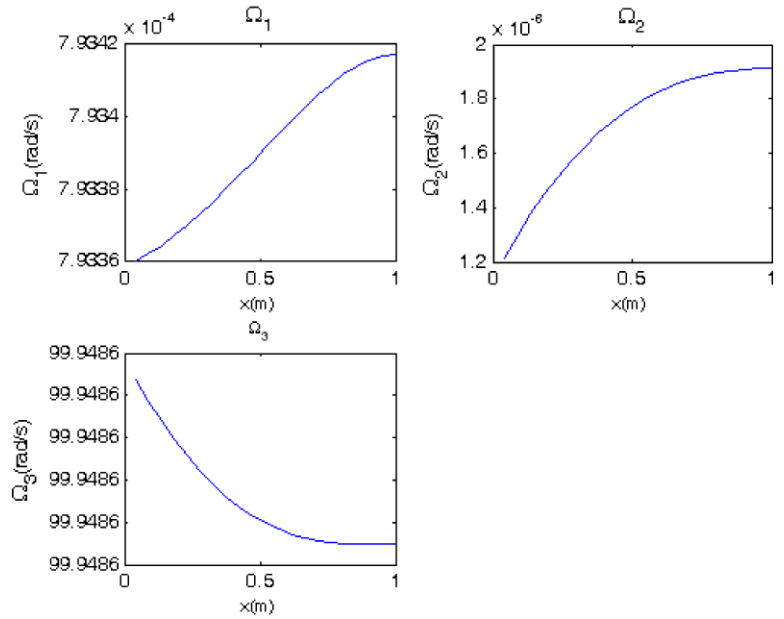

Fig. 22 Variation of blade angular velocity components along its span at $t = 0.85$ s

8.3 Case study: damped elastic composite airfoil

Consider the case of a composite airfoil similar to what is discussed in Cesnik et al. [5]. The UM/VABS input file for this case is among the examples provided with the software. The airfoil is a NACA 4415 airfoil with double-cells and has a spar located at 38.6% chord from the leading edge as is shown in Fig. 23.

The position of the centroid is at $y = 0.3084$ m and $z = 0.06210$ m. Figure 24 illustrates the ply lay-up definitions and orientation angles on the section. A passive 0° ply is used to enclose the cross section. The inner layers consist of 90°, +45°, −45° and 0°

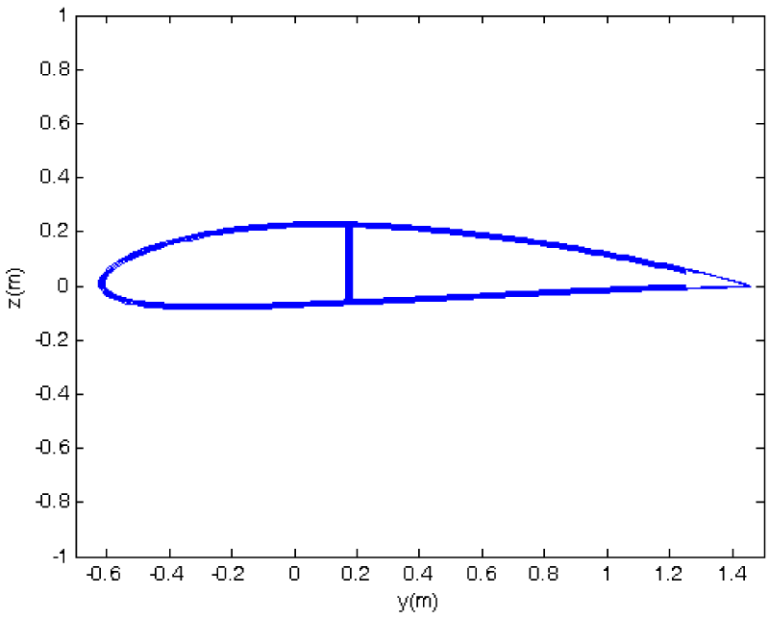

Fig. 23 Cross section of the airfoil

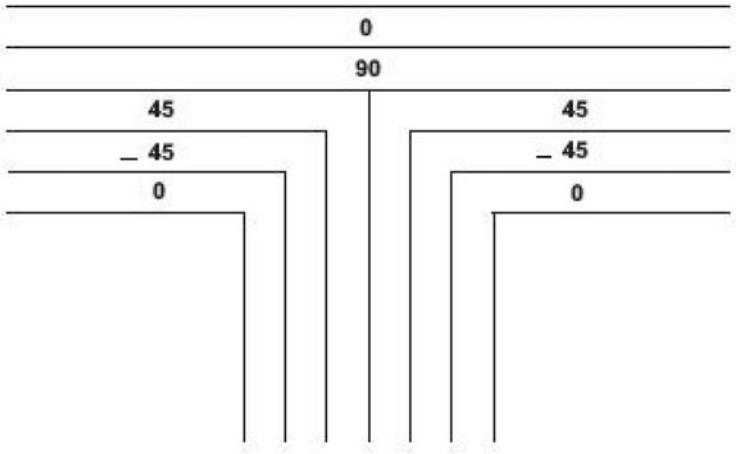

Fig. 24 Ply layups and orientation angles of the airfoil cross section [5]

active plies (i.e. $[0, +90, +45, -45, 0]$). The angles are measured with respect to the axis along the wing span.

Using the material properties given in Cesnik et al. [5] and implementing UM/VABS, the stiffness matrix of the cross section is obtained as

$$S = \begin{bmatrix} 1.12577 \times 10^9 & 3.615437 \times 10^3 & -1.28217 \times 10^4 & -1.64732 \times 10^5 & -2.168324 \times 10^5 & -5.681057 \times 10^6 \\ 3.615437 \times 10^3 & 3.15555 \times 10^8 & -4.04582 \times 10^5 & -1.0509 \times 10^7 & 7.05125 \times 10^4 & 4.33983 \times 10^3 \\ -1.28217 \times 10^4 & -4.04582 \times 10^5 & 2.79485 \times 10^7 & -1.06215 \times 10^7 & 5.81197 \times 10^2 & 1.08681 \times 10^4 \\ -1.64732 \times 10^5 & -1.0509 \times 10^7 & -1.06215 \times 10^7 & 1.75149 \times 10^7 & -2.4470 \times 10^3 & 2.00316 \times 10^3 \\ -2.168324 \times 10^5 & 7.05125 \times 10^4 & 5.81197 \times 10^2 & -2.4470 \times 10^3 & 1.39200 \times 10^7 & 1.16753 \times 10^5 \\ -5.681057 \times 10^6 & 4.33983 \times 10^3 & 1.08681 \times 10^4 & 2.00316 \times 10^3 & 1.16753 \times 10^5 & 3.3672 \times 10^8 \end{bmatrix}$$

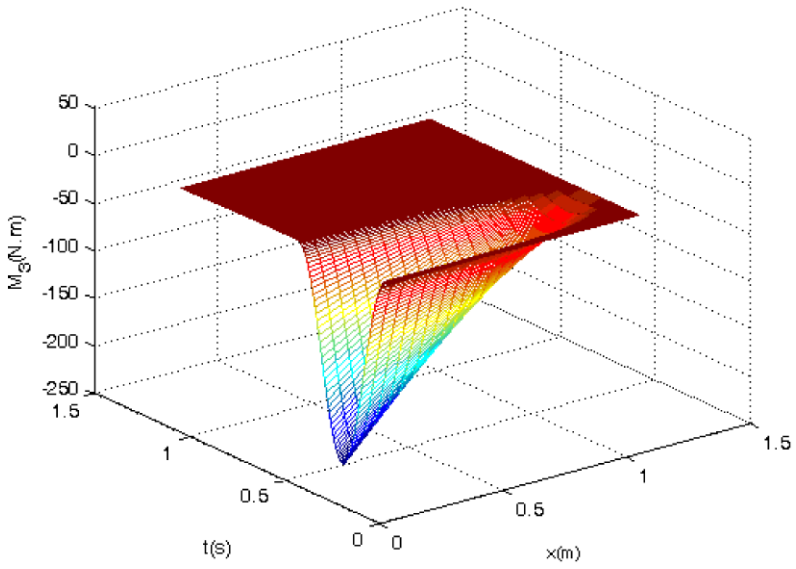

Fig. 25 Time history diagrams of beam internal moment components at the root

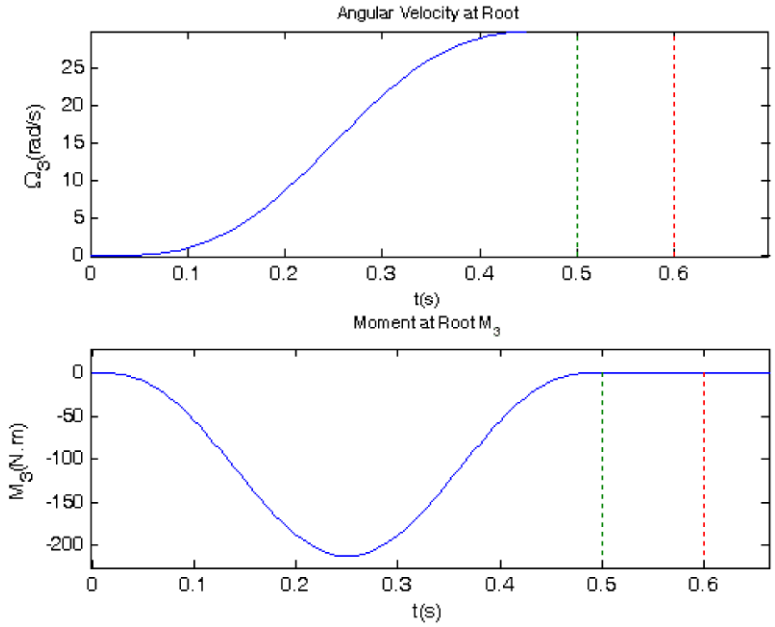

Fig. 26 Time history diagrams of shaft angular velocity and the M_3 bending moment induced in the beam at the root

Figures 25, 26, 27, 28 and 30 illustrate the solution for the full speed angular velocity of 30 rad/s, a 4% hinge offset ratio, unit applied moments in the 2 and 3 directions and using

$$I = \begin{bmatrix} 77.255 & 0 & 0 \\ 0 & 3.1362 & -0.20052 \\ 0 & -0.20052 & 74.119 \end{bmatrix} \times 10^{-2}$$

9 Conclusions

A direct integration method which utilizes the perturbation method was presented for the elasto-dynamic analysis of an accelerating articulated composite blade. The solution involves the application of the Variational-Asymptotic Method (VAM) and calculation of the cross-sectional properties of the elastic blade as well as solving the nonlinear intrinsic differential equations of motion of the blade. A generalized solu-

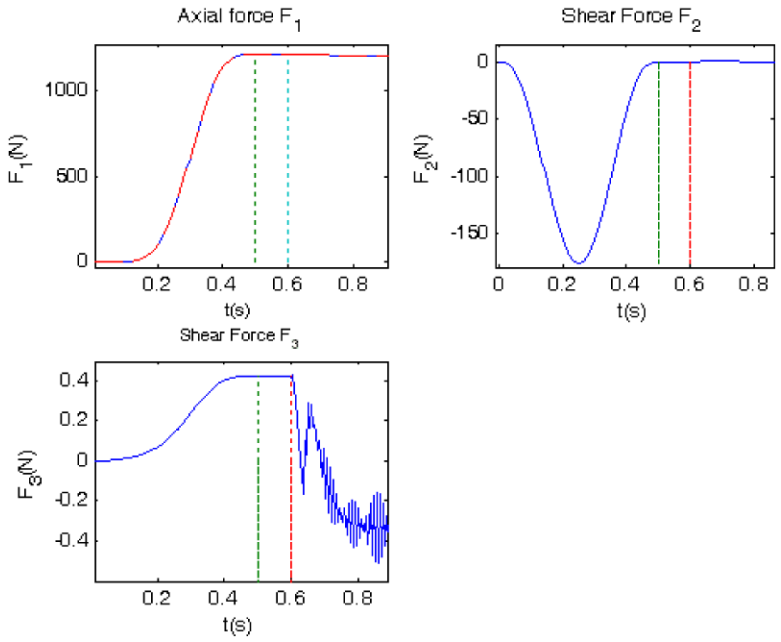

Fig. 27 Time history diagrams of beam internal force components at the root; present solution (*solid line*) (70) (*dashed line*)

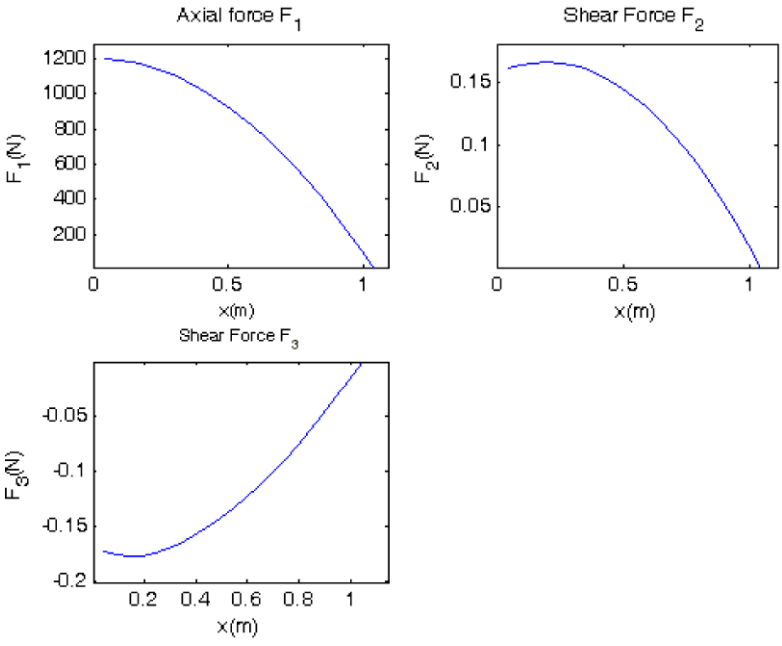

Fig. 28 Variation of beam internal force components along its span at $t = 0.85$ s

tion to the coupled rigid-body motion problem of helicopter blades in flap and lead-lag was also derived and used in order to generate the root boundary conditions. Using this solution, an algorithm was developed and implemented in order to calculate the transient and the steady-state solutions of the intrinsic differential equations of motion including internal forces, moments, velocities and angular velocities. The specific problem considered involved an accelerating rotor blade that started its motion from rest and converged to a steady-state angular velocity. The solution was shown to be in good agreement with the linear solution for the axial force as well as with the imposed boundary conditions. The resulting simulation code is a powerful

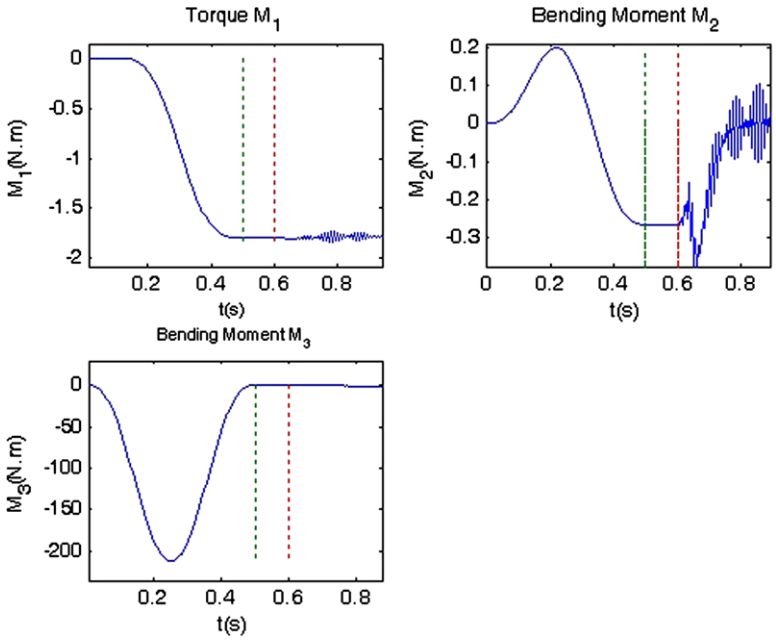

Fig. 29 Time history diagrams of beam internal moment components at the root

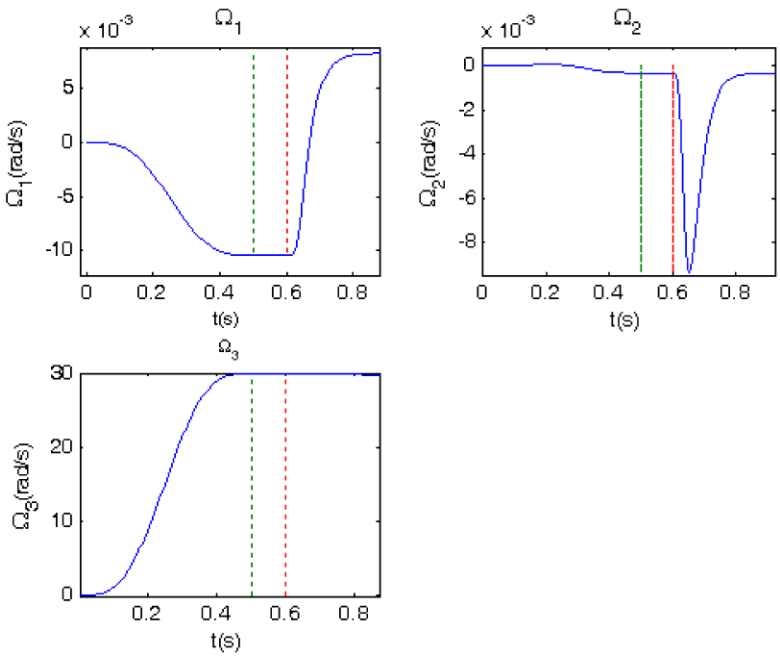

Fig. 30 Time history diagrams of beam angular velocity components at the root

tool for analyzing the nonlinear response of composite rotor blades; and can be used in the future for reaching the ultimate aim of efficient noise and vibration control of helicopters.

Acknowledgements The author is grateful to Professors Dewey H. Hodges and Fred Nitzsche for their constructive comments. He also appreciates the helpful suggestions made by two anonymous reviewers. The Alexander Graham Bell Canada Graduate Scholarship Award by the Natural Science and Engineering Research Council of Canada and the J.Y. and E.W. Wong Research Award in Mechanical/Aerospace Engineering to the author supported this research and are gratefully acknowledged.

References

1. Berdichevsky, V.L.: On the energy of an elastic rod. Prikl. Mat. Meh. **45**, 518–529 (1981)
2. Berdichevsky, V.L., Armanios, E.A., Badir, A.M.: Theory of anisotropic thin-walled closed cross section beams. Compos. Eng. **2**, 411–432 (1992)
3. Cesnik, C.E.S., Ortega-Morales, M.: Active composite beam cross-sectional modeling—stiffness and active force constraints. In: 40th AIAA/ASCE/AHS/ASC Structures, Structural Dynamics, and Materials Conference, St. Louis, MO, 12–15 April (1999). Paper No.: AIAA-99-1548
4. Cesnik, C.E.S., Ortega-Morales, M.: Active beam cross-sectional modeling. J. Intell. Mater. Syst. Struct. **12**, 483–496 (2001)
5. Cesnik, C.E.S., Park, R.S., Palacios, R.: Effective cross-section distribution of anisotropic piezocomposite actuators for wing twist. Proc. SPIE **5056**, 21–32 (2003)
6. Cesnik, C.E.S., Shin, S.J.: Structural analysis for designing rotor blades with integral actuators. In: 39th AIAA/ASME/ASCE/ASC Structures, Structural Dynamics, and Materials Conference, Long Beach, CA, 20–23 April (1998). Paper No.: AIAA-98-2107
7. Done, G., Balmford, D.: Bramwell's Helicopter Dynamics, 2nd edn. AIAA, Washington (2001)
8. Esmailzadeh, E., Ghorashi, M.: Vibration analysis of a Timoshenko beam subjected to a traveling mass. J. Sound Vib. **199**(4), 615–628 (1997)
9. Ghorashi, M.: Dynamic and vibratory analysis of beams under dynamic loads induced by traveling masses and vehicles. Ph.D. thesis, Mechanical Engineering Department, Sharif University of Technology (1994)
10. Ghorashi, M., Nitzsche, F.: Steady state nonlinear dynamic response of a composite rotor blade using implicit integration of intrinsic equations of a beam. Int. Rev. Aerosp. Eng. **1**, 225–233 (2008)
11. Ghorashi, M.: Dynamics of elastic nonlinear rotating composite beams with embedded actuators. Ph.D. thesis, Mechanical and Aerospace Engineering Department, Carleton University (2009)
12. Ghorashi, M., Nitzsche, F.: Nonlinear dynamic response of an accelerating composite rotor blade using perturbations. J. Mech. Mater. Struct. **4**, 693–718 (2009)
13. Hodges, D.H., Atilgan, A.R., Cesnik, C.E.S., Fulton, M.V.: On a simplified strain energy function for geometrically nonlinear behavior of anisotropic beams. Compos. Eng. **2**, 513–526 (1992)
14. Hodges, D.H., Shang, X., Cesnik, C.E.S.: Finite element solution of nonlinear intrinsic equations for curved composite beams. J. Am. Helicopter Soc. **41**, 313–321 (1996)
15. Hodges, D.H.: Nonlinear Composite Beam Theory. AIAA, Washington (2006)
16. Hopkins, A.S., Ormiston, R.A.: An examination of selected problems in rotor blade structural mechanics and dynamics. In: Proceedings of the 59th American Helicopter Society Forum, Phoenix, AZ (2003)
17. Johnson, W.: Helicopter Theory. Dover, New York (1994)
18. Leishman, J.G.: Principles of Helicopter Aerodynamics, 2nd edn. Cambridge University Press, New York (2006)
19. Shang, X., Hodges, D.H.: Aeroelastic stability of composite rotor blades in hover. In: 36th Structures, Structural Dynamics and Materials Conference, New Orleans (1995). Paper No: AIAA-95-1453-CP
20. Sharpe, D.L.: An experimental investigation of the flap-lag-torsion aeroelastic stability of a small-scale hingeless helicopter rotor in hover. NASA, TP-2546 (1986)
21. Yu, W., Volovoi, V.V., Hodges, D.H., Hong, X.: Validation of the variational asymptotic beam sectional analysis. AIAA J. **40**, 2105–2112 (2002)
22. Yu, W., Hodges, D.H.: Elasticity solutions versus asymptotic sectional analysis of homogeneous, isotropic, prismatic beams. J. Appl. Mech. **71**, 15–23 (2004)